Far-infrared absorption of interaction-induced ground states of two weakly coupled quantum wires

C. Steinebach and D. Heitmann
Institut für Angewandte Physik und Zentrum für Mikrostrukturforschung, Jungiusstraße 11, 20355 Hamburg, Germany

Vidar Gudmundsson
Science Institute, University of Iceland, Dunhaga 3, IS-107 Reykjavik, Iceland
(Received 29 May 1998)

We theoretically investigate the far-infrared (FIR) absorption of two weakly coupled vertical $GaAs/Al_xGa_{1-x}As$ quantum wires subjected to a perpendicular magnetic field. The calculations are performed within the time-dependent Hartree-Fock approximation. For a single occupied subband we find, depending on the electron density, different interaction-induced ground states. For small densities the interlayer exchange energy dominates, and we find a symmetric ground state with strong interlayer coherence. For larger densities the interplay of direct and exchange interaction drives the system into a state that shows the characteristics of a charge-density wave (CDW) in the direction of lateral confinement. The signatures of these states, the exchange enhanced tunneling gap of the coherent state and the density oscillations of the CDW, are directly reflected in the FIR spectrum. [S0163-1829(98)01743-3]

I. INTRODUCTION

Double-layered two-dimensional electron systems (2DES's) are currently a subject of growing interest. Much theoretical [1–7] and experimental[8–10] work has been carried out investigating the possible existence of exchange-correlation-driven broken-symmetry ground states in such systems. Even in the absence of any tunneling the interaction may lead to a ground state with spontaneous interlayer phase coherence.[3,6,7] Exact finite-size numerical calculations for a filling fraction $\nu=1$ predict different incompressible quantum Hall states driven either by the single-particle tunneling gap Δ^0_{SAS} or by the electron-electron interaction.[11] Both states were experimentally observed.[12] Calculations within the Hartree-Fock approximation (HFA) show that at $\nu=1$ a double-layered 2DES can lower its energy by spontaneously breaking its translational invariance.[13] At certain values for the ratio of layer separation and magnetic length, the uniform coherent state becomes instable against the formation of either a charge-density wave (CDW) or a Wigner-crystal state.

In this work we investigate the ground state and the far-infrared (FIR) absorption of two weakly coupled vertical quantum wires for magnetic fields where one or two spin-split one-dimensional (1D) subbands are occupied ($\nu=1$ and 2). We work in the regime of intermediate layer separations $D+w\approx 15$ nm, where the unrenormalized tunneling gap is small ($\Delta^0_{SAS}\approx 0.15$ meV). D is the barrier thickness and w the thickness of the quantum wires in the growth direction z (see Fig. 1). Exact numerical calculations for quantum dots show that for these layer separations the interlayer correlations are small.[14] We consider the layers to have slightly different external potentials, an effect that is present in any actual sample. Electrostatics show that the difference in the confinement energies is of the order of 10%.[15] Depending on the electron density we find different ground states at $\nu=1$. For small densities the ground state is a coherent tunneling-dominated state where the single-particle states form symmetric and antisymmetric combinations of wave functions located in the isolated wires. For larger densities we find a transition to a CDW-like state where the electron densities in the two wires are modulated in the lateral direction and shifted by half a wavelength against each other in order to reduce the interlayer Hartree repulsion. As pointed out in Ref. 13, the CDW is at the cost of interlayer exchange energy, but it optimizes the intralayer exchange energy by accumulating electrons in regions with a width of about two magnetic lengths l_c. Only in this region does the exchange give a significant contribution. In quantum wires the CDW is additionally stabilized by the different confinement energies. The dependence of the ground state on the interlayer separation D is more complicated than for the 2D case, where the transition to the CDW is found at $D/l_c\approx 1.5$. In particular, we do not find a CDW for sufficiently small electron densities by increasing D and keeping l_c fixed. A large D reduces the interlayer screening, and therefore the width of the electron distribution shrinks. When the width becomes smaller than the wavelength of the CDW $\lambda_{CDW}\approx 4l_c$, the formation of the CDW is counteracted by the external confinement. However, there is still the possibility of a longitudinal CDW which we do not consider.

We calculate the FIR absorption of such a system within the time-dependent HFA (TDHFA). The characteristics of the different ground states can be found in the calculated spectra. In particular, the low-density coherent state has an acoustic intersubband magnetoplasmon mode with a higher frequency than the optical one. We will show that this is a direct evidence of the enhancement of the tunneling gap.[16] In systems without tunneling the acoustic mode is usually found below the optical one.[17,18]

The TDHFA has been selected in light of the close fit obtained to experimental results for collective charge- and spin-density excitations in quantum wires.[19,20] We are aware of the fact that the TDHFA cannot properly describe corre-

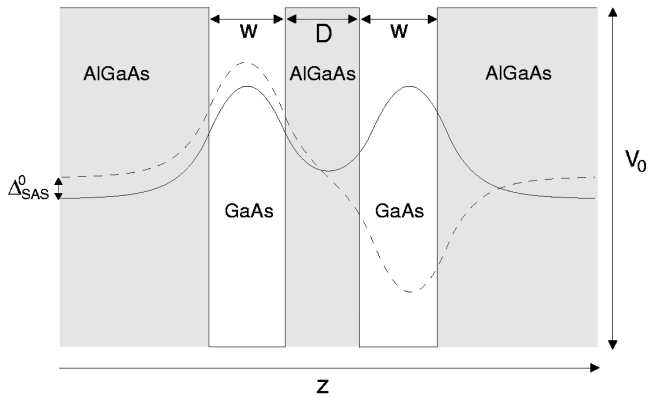

FIG. 1. Sketch of a double-layered quantum-well structure. The two GaAs layers are separated by a distance D, and each well has a width w. The band-gap offset between GaAs and $Al_xGa_{1-x}As$ is V_0. The single-particle wave functions of the lowest subbands are indicated as solid (ground state) and dashed (first excited state) lines. In the absence of the exchange interaction the states are separated by the pure tunneling gap Δ^0_{SAS}.

lation effects beyond a simple spin correlation. Thus we can not predict precisely the parameter range where broken-symmetry ground states occur.

II. MODEL

A schematic cross section of the underlying double quantum well in the growth direction z is shown in Fig. 1. The widths of the GaAs quantum wells and of the $Al_xGa_{1-x}As$ barrier that separates the two electron systems are w and D, respectively. Also indicated are the band-gap offset V_0 and the wave functions of the two lowest 2D subbands which are separated in energy by the tunneling gap Δ^0_{SAS}.

We treat the electron-electron interaction in the HFA, and account approximately for the finite thickness of the wires in the z direction as described below. The lateral direction and the direction along the wires are chosen as the y and x directions, respectively. We assume the lateral confinement to be parabolic with different confinement energies $\hbar\omega_0^\lambda$ in the two sheets. The index $\lambda = l,r$ denotes the left and right wires, respectively. We consider a magnetic field $\mathbf{B}$ in the z direction with the vector potential in Landau gauge $\mathbf{A} = (-yB,0,0)$. The single-electron states are written as two-component spinors

$$\psi_{\mu k\sigma}(x,y) = \frac{1}{\sqrt{L_x}} e^{ikx} \begin{bmatrix} \varphi^l_{\mu k\sigma}(y) \\ \varphi^r_{\mu k\sigma}(y) \end{bmatrix}, \tag{1}$$

where L_x is the length of the wire, μ is the subband index, k is the longitudinal quantum number, σ is the spin index, and $l(r)$ refer to the part of the wave function which is located in the left (right) quantum wire, respectively. The single-particle states are solutions of the HF equation

$$\begin{bmatrix} H^{ll}_{k\sigma} & H^{lr}_{k\sigma} \\ H^{rl}_{k\sigma} & H^{rr}_{k\sigma} \end{bmatrix} \begin{bmatrix} \varphi^l_{\mu k\sigma} \\ \varphi^r_{\mu k\sigma} \end{bmatrix} = \epsilon_{\mu k\sigma} \begin{bmatrix} \varphi^l_{\mu k\sigma} \\ \varphi^r_{\mu k\sigma} \end{bmatrix}. \tag{2}$$

The Hamiltonian is given by $H_{k\sigma} = H_{0,k} + H_{Z,\sigma} + H_T + H_H + H_{F,k\sigma}$. $H_{0,k}$ describes the kinetic energy and the external potential

$$H^{\lambda\lambda'}_{0,k} = \delta_{\lambda\lambda'} \left[-\frac{\hbar^2}{2m^*}(\partial_y^2 - k^2) + \frac{1}{2} m^* (\omega_0^{\lambda 2} + \omega_c^2) y^2 - \hbar\omega_c k y \right], \tag{3}$$

with the effective mass of GaAs $m^* = 0.07 m_0$ and the cyclotron frequency $\omega_c = eB/m^*$.

H_T and H_Z describe the tunneling and Zeeman energy:

$$H^{\lambda\lambda'}_{Z,\sigma} = \delta_{\lambda\lambda'} g^* \mu_B B \sigma, \tag{4}$$

$$H_T = -\frac{\Delta^0_{SAS}}{2} \begin{bmatrix} 0 & 1 \\ 1 & 0 \end{bmatrix}. \tag{5}$$

The g factor of GaAs is $g^* = -0.44$, μ_B is the Bohr magneton, and $\sigma = \pm\frac{1}{2}$. We calculate Δ^0_{SAS} by solving the Schrödinger equation of the underlying quantum-well structure in the growth direction z. The Hartree potential is

$$H^{\lambda\lambda'}_H(y) = \delta_{\lambda\lambda'} \sum_{\lambda''} \int dy' \rho^{\lambda''}(y') v^{\lambda\lambda''}(|y-y'|), \tag{6}$$

where the intralayer and interlayer interactions are

$$v^{\lambda\lambda''}(|y-y'|) = -\frac{e^2}{2\pi\epsilon\epsilon_0} \ln \sqrt{\frac{(y-y')^2 + (w/2)^2}{L^2}} \quad \text{for} \quad \lambda = \lambda'' \tag{7}$$

and

$$v^{\lambda\lambda''}(|y-y'|) = -\frac{e^2}{2\pi\epsilon\epsilon_0} \ln \sqrt{\frac{(y-y')^2 + (D+w)^2}{L^2}} \quad \text{for} \quad \lambda \neq \lambda''. \tag{8}$$

$\epsilon = 12.53$ is the dielectric constant of GaAs, L is an arbitrary length, and w accounts approximately for the finite thickness of the wires in z direction. The electron density in wire λ is

$$\rho^\lambda(y) = \frac{1}{L_x} \sum_{\mu k\sigma} f_{\mu k\sigma} |\varphi^\lambda_{\mu k\sigma}(y)|^2. \tag{9}$$

$f_{\mu k\sigma}$ is the Fermi occupation number of the state $|\mu k\sigma\rangle$. The exchange part of the Hamiltonian is in general nondiagonal in the layer index

$$(H^{\lambda\lambda'}_{F,k\sigma}\varphi^{\lambda'}_{\mu k\sigma})(y) = \sum_{\mu' k'} f_{\mu' k'\sigma} \varphi^\lambda_{\mu' k'\sigma}(y) \times \int dy' \varphi^{\lambda'*}_{\mu' k'\sigma}(y') \varphi^{\lambda'}_{\mu k\sigma}(y') \times K^{\lambda\lambda'}_{kk'}(|y-y'|), \tag{10}$$

with

$$K_{kk'}^{\lambda\lambda'}(|y-y'|) = -\frac{e^2}{2\pi\epsilon\epsilon_0 L_x} K_0[|k-k'| \times \sqrt{(y-y')^2+(w/2)^2}] \quad \text{for} \quad \lambda=\lambda', \quad (11)$$

and

$$K_{kk'}^{\lambda\lambda'}(|y-y'|) = -\frac{e^2}{2\pi\epsilon\epsilon_0 L_x} K_0[|k-k'| \times \sqrt{(y-y')^2+(D+w)^2}] \quad \text{for} \quad \lambda\neq\lambda'. \quad (12)$$

K_0 is a modified Bessel function which has a logarithmic singularity at $k=k'$. This is treated by remembering that in the long-wire limit the k sums are replaced by integrals. As the singularity is logarithmic, it can be integrated.

We search for a self-consistent solution of Eq. (2). It turns out that for certain magnetic fields we end up with a small number of different solutions of Eq. (2) depending on the state we started the iterative procedure with. In order to decide which one is the HF ground state we started our iteration with different values of Δ_{SAS}^0 and g^* which were finally set to their actual values. Then we calculated the total energy E_t of the different solutions according to the formula

$$E_t = \sum_a f_a \epsilon_a - \tfrac{1}{2}\sum_{ab} f_a f_b [\langle ab|v|ab\rangle - \langle ab|v|ba\rangle], \quad (13)$$

with v being the 3D Coulomb interaction, and we have defined combined quantum numbers $a=(\mu,k,\sigma)$, $b=(\mu',k',\sigma')$.

The FIR absorption for an external potential $\Phi_{ext}=-yE_{ext}$ is calculated within the TDHFA (Ref. 21) from the Joule heating of the system,

$$P(\omega) = \frac{1}{2}\sum_\lambda \int d^2r \Re[\delta\mathbf{j}^\lambda(\mathbf{r},\omega)\mathbf{E}^{\lambda *}(\mathbf{r},\omega)]. \quad (14)$$

$\delta\mathbf{j}^\lambda(\mathbf{r},\omega)$ is the induced current density and $\mathbf{E}^\lambda(\mathbf{r},\omega)$ the total self-consistent (SC) electric field. P can be written as

$$P(\omega) \propto \omega E_{ext} \sum_{ab} \langle b|y|a\rangle \Im[f_{ab}(\omega)\langle a|\Phi^{SC}|b\rangle], \quad (15)$$

The matrix elements of the self-consistent potential Φ^{SC} are found as the solution of the linear set of equations

$$\sum_{dc} \epsilon_{ab,dc}(\omega)\langle d|\Phi^{SC}|c\rangle = \langle a|\Phi^{ext}|b\rangle, \quad (16)$$

with the dielectric tensor

$$\epsilon_{ab,dc}(\omega) = [\delta_{ab,dc} - (H_{cd,ba}+F_{cd,ba}) f_{dc}(\omega)], \quad (17)$$

where

$$H_{cd,ba} = \frac{1}{L_x}\sum_{\lambda\lambda'} \int dy\, dy' \varphi_c^{\lambda *}(y) \times \varphi_d^\lambda(y)\varphi_a^{\lambda' *}(y')\varphi_b^{\lambda'}(y') v^{\lambda\lambda'}(|y-y'|), \quad (18)$$

$$F_{cd,ba} = \sum_{\lambda\lambda'} \int dy dy' \varphi_c^{\lambda *}(y)\varphi_d^{\lambda'}(y') \times \varphi_a^{\lambda' *}(y')\varphi_b^\lambda(y) K_{kk'}^{\lambda\lambda'}(|y-y'|), \quad (19)$$

$$f_{dc}(\omega) = \frac{f_d - f_c}{\epsilon_d - \epsilon_c - \hbar\omega - i\gamma}. \quad (20)$$

γ is a phenomenological broadening.

III. RESULTS AND DISCUSSION

Let us first consider a system with a small electron density $n_{1D}=4\times10^5$ cm^{-1}. For a magnetic field of $B=3.3$ T only the lowest spin-split 1D subband is populated. The confinement energies are $\hbar\omega_0^l=4$ meV and $\hbar\omega_0^r=4.2$ meV, and the tunneling gap is $\Delta_{SAS}^0=0.16$ meV for an aluminum concentration of $x=0.35$. The subband dispersion is displayed in Fig. 2(a). For these parameters we find that the single-particle states can be classified to a good approximation as pairs of symmetric and antisymmetric states. We label the subbands by is and ia, where i is the lateral quantum number, and s and a refer to the symmetric and antisymmetric states, respectively. Figure 2(b) shows the probability of an electron in the considered subbands to be located in the layer $\lambda=l$. We find two different regions. For small values of k, which corresponds to states located in the center of the wire, the tunneling is nearly perfect, whereas states at the edge of the wire are more located in either one of the layers. The bare tunneling gap Δ_{SAS}^0 is enhanced by the nonlocal interlayer exchange interaction. This is similar to the effect of the enhanced g factor.[22] As the chemical potential μ lies between the bands $1s$ and $1a$, the symmetric states are lowered in energy by the interlayer exchange self-energy. For the enhanced tunneling gap we find at $k=0$ $\Delta_{SAS}^*=5.4$ meV for $i=1$ and $\Delta_{SAS}^*=1.2$ meV for $i=2$. Thus this coherent tunneling-dominated ground state is stabilized by taking advantage of the interlayer exchange energy. The density distribution in the two wires is shown in Fig. 2(c). As for a single wire it has its maximum in the center.

The FIR absorption of this state is depicted in Fig. 3(a). We find three major peaks. The resonances $\omega_o^{(1)}$ and $\omega_o^{(2)}$ are optical modes, as can be seen from the induced density oscillations shown in Fig. 3(b). The mode labeled ω_a is an acoustic mode as it corresponds to an out-of-phase motion of the electrons. There are two interesting features which are the signature of the underlying ground state. First, the optical mode splits into two peaks. We will explain later that $\omega_o^{(1)}$ is an edge plasmon whereas $\omega_o^{(2)}$ is due to an oscillation in the

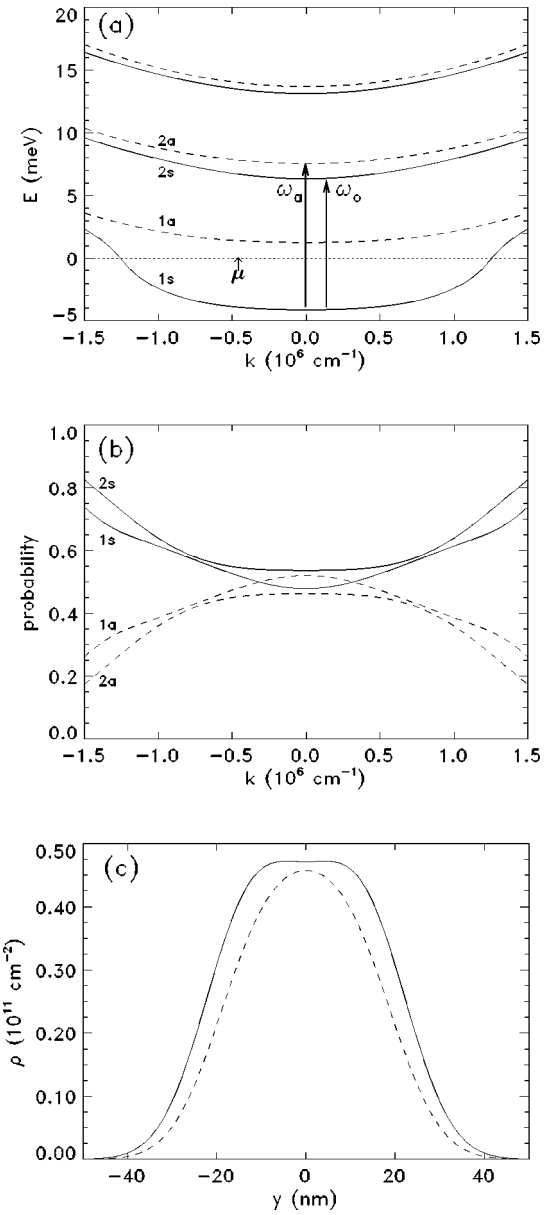

FIG. 2. 1D subbands with $\sigma=\frac{1}{2}$ (a), probability of a state to be located in the left wire (b), and the ground-state density (c) of weakly coupled vertical quantum wires at $B=3.3$ T. The electron densities are $n_{1D}=4\times10^5$ cm^{-1}, $x=0.35$, and $\Delta^0_{SAS}=0.16$ meV, and the confinement energies $\hbar\omega_0^l=4$ meV and $\hbar\omega_0^r=4.2$ meV. The chemical potential in (a) is set to $\mu=0$. In (c) the solid line shows the density in wire $\lambda=l$, and the dashed line the density in layer $\lambda=r$.

bulk region of the wire. Even more interesting is the fact that ω_a is higher in energy than the optical mode. This directly reflects the effect of the enhanced tunnel gap. In systems with no tunneling we always have $\omega_o>\omega_a$ due to the reduced depolarization shift of the acoustic mode.[18] As the acoustic mode is connected with an out-of-phase motion of the electrons in the two layers, it corresponds to transitions $1s\rightarrow2a$, as indicated in Fig. 1(a). The optical modes are mainly due to transitions $1s\rightarrow2s$. The effect of interlayer exchange which shifts ω_a to higher values is not compensated for by dynamical vertex corrections, i.e. the exciton shift. These are nearly the same for both transitions. This can

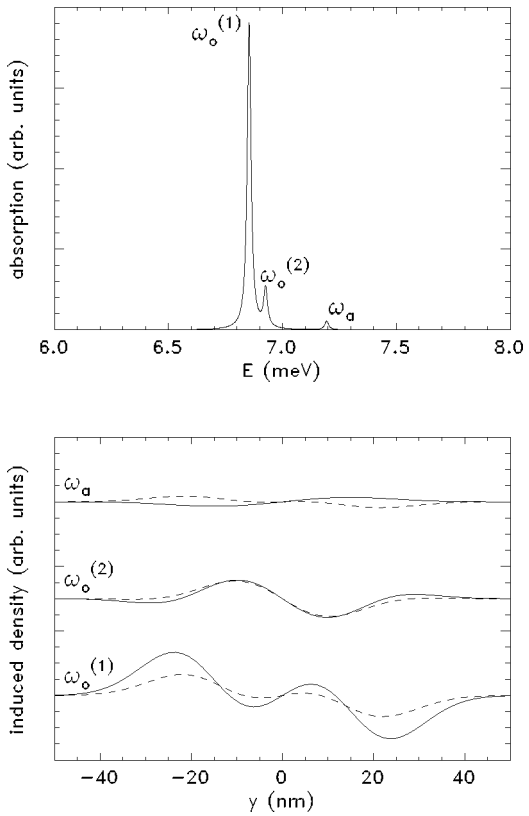

FIG. 3. FIR spectrum (upper figure) and induced charge density (lower figure) calculated for the same parameters as used in Fig. 2. The optical modes are labeled as $\omega_o^{(i)}$, and the acoustic mode as ω_a. In the lower figure the solid lines correspond to layer $\lambda=l$, the dashed lines to $\lambda=r$.

be easily derived from Eq. (19). The main contribution to the transition $1s\rightarrow2a$ is due to the diagonal matrix element $F_{1s2ak\sigma,1s2ak'\sigma}$. For a symmetric system this is exactly the same as $F_{1s2sk\sigma,1s2sk'\sigma}$ which is prominent for the transition $1s\rightarrow2s$. Furthermore, as we are in the low-density regime, the depolarization effect is small. As a net result of reduced depolarization shift and enhanced tunnel gap we find $\omega_a>\omega_o$.

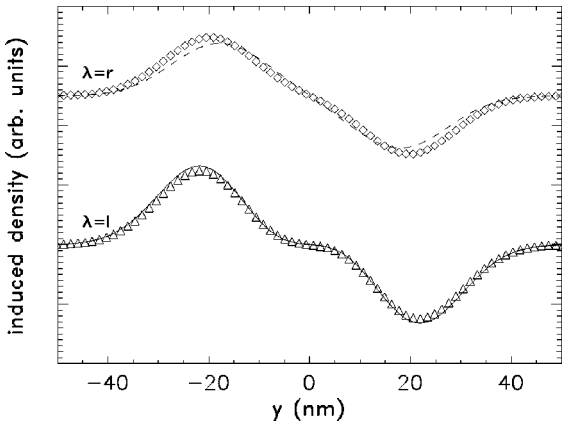

FIG. 4. Sum of the induced density of the modes $\omega_o^{(1)}$ and $\omega_o^{(2)}$. The solid and dashed lines refer to the parameters of Fig. 3, the open triangles and diamonds to $\hbar\omega_0^r=4.1$ meV.

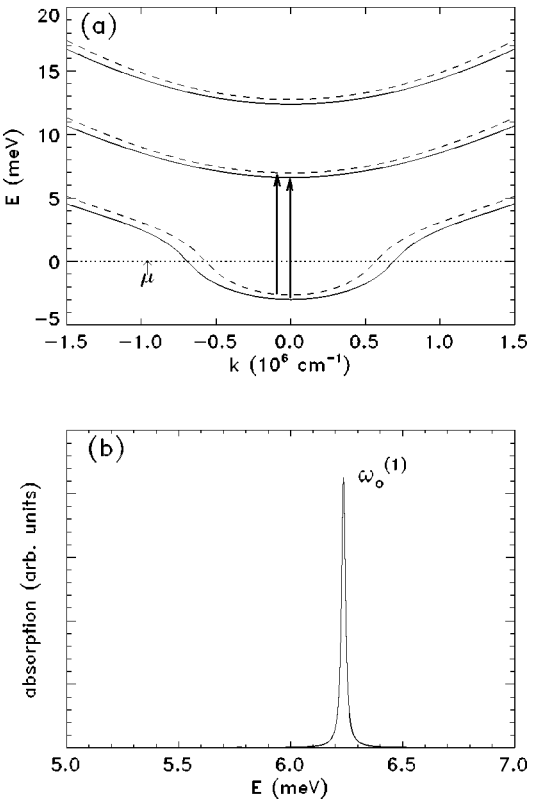

FIG. 5. Subbands (a) and FIR absorption (b) for $B=2.8$ T. The other parameters are the same as in Fig. 2. In (a) the solid lines correspond to states which are mostly localized in layer $\lambda=l$, and the dashed lines to states in layer $\lambda=r$. The arrows indicate the allowed single-particle transitions.

The splitting of the optical mode is a combined effect of tunneling and different confinement potentials in the two wires. From the induced density in Fig. 3(b) we can deduce that $\omega_o^{(2)}$ is caused by transitions in the center of the wire. The node structure of $\omega_o^{(1)}$ implies that it consists of transitions at the edge of the wire. This can be understood from Fig. 2(b). In k space there are two different regions. For small k the electrons occupy symmetric and antisymmetric states. For increasing k these states are eventually destroyed as the potential difference increases for states localized at the edge. Thus, we find two groups of single-particle states, each participating predominantly in a collective plasmon mode.

In order to confirm this picture we have calculated the FIR spectrum for $\hbar\omega_0^l=4$ meV and $\hbar\omega_0^r=4.1$ meV. For $\hbar\omega_0^l\rightarrow\hbar\omega_0^r$ the two optical peaks eventually merge and the high-energy mode decreases in intensity. The additional oscillations in the induced density of the $\omega_o^{(1)}$ mode disappear. These oscillations were due to a lack of transitions near $k=0$ which are now redistributed from the $\omega_o^{(2)}$ mode.

Figure 4 shows the sum of the induced densities of the two optical modes. The lines are calculated for $\hbar\omega_0^r=4.2$ meV, and the open symbols for $\hbar\omega_0^r=4.1$ meV. Although the individual oscillations are quite different for the two cases, the sums are nearly identical. Only for $\lambda=r$ does the distribution become slightly wider for $\hbar\omega_0^r=4.1$ meV due to the decreasing confinement. This additionally stresses our statement that the two optical peaks are due to different

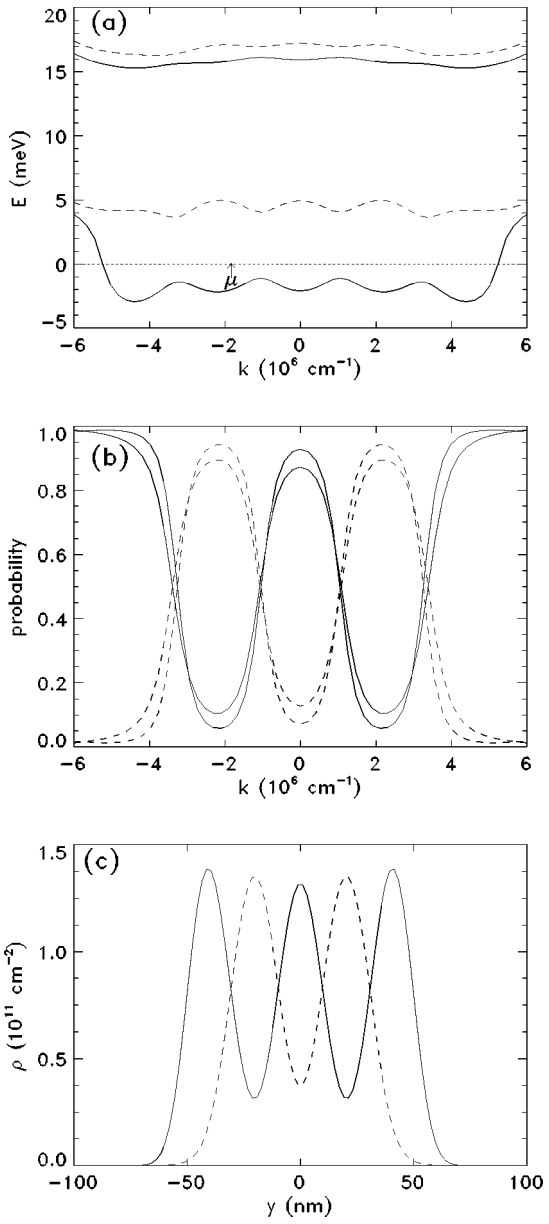

FIG. 6. Subband dispersion (a), probability of a single-particle state to be located in layer $\lambda=l$ (b), and ground-state density (c) for a pair of quantum wires at $B=7$ T and $n_{1D}=1.7\times10^6$ cm^{-1}. The other parameters are the same as in Fig. 2. The solid (dashed) lines in (b) correspond to solid (dashed) lines in (a). In (c) the solid line shows the density in wire $\lambda=l$, and the dashed line the density in wire $\lambda=r$.

groups of transitions in k space. The question of which transition contributes to which mode depends on the degree of asymmetry between the wires and the tunneling strength.

We compare the absorption of the tunneling dominated state described above with that for a lower magnetic field $B=2.8$ T. Figure 5 displays the subbands and the calculated FIR spectrum. Two subbands are occupied which are dominantly localized in the left (solid lines) and the right (dashed lines) wires, respectively. The arrows indicate the allowed transitions. The collective excitations correspond to in-phase coupling (optical mode) and out-of-phase coupling (acoustic mode) of these transitions. The acoustic mode carries very

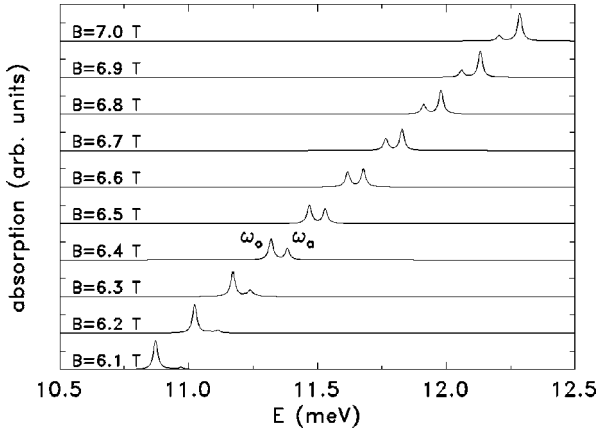

FIG. 7. FIR absorption as a function of the magnetic field for the same parameters as in Fig. 6.

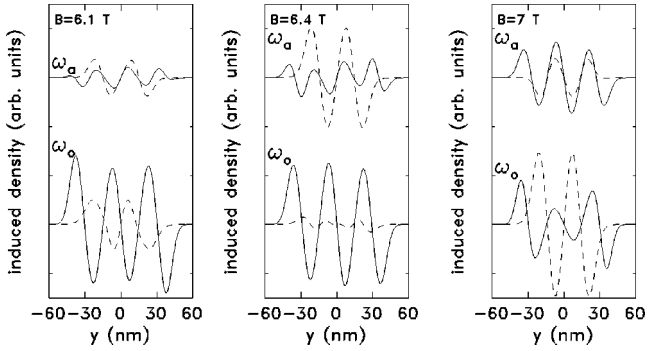

FIG. 8. Induced densities in layer $\lambda = l$ (solid line) and $\lambda = r$ (dashed line) for magnetic fields $B = 6.1$, 6.4, and 7 T.

little oscillator strength and is not resolved in Fig. 5(b). The crossover from this state to the tunneling-dominated state takes place abruptly at $B = 3.1$ T, when the coherent state becomes lower in energy. We do not observe a continuous transition between these two states.

Recently, double-layered 2DES at $\nu = 2$ have attracted much interest due to a phase with interlayer in-plane antiferromagnetic spin correlations that is expected to occur at intermediate tunneling gaps Δ^0_{SAS}.[4] Since we are interested in the regime of small tunneling, the system considered in our work is in the ferromagnetic region of the phase diagram calculated in Ref. 4. Therefore, we do not perform an unrestricted HFA with respect to the spin-degree of freedom which would be necessary to account for the antiferromagnetic phase.

We now investigate the situation of larger electron density $n_{1D} = 1.7 \times 10^6$ cm^{-1}, but the same values for the external potential as in Fig. 2. The subband dispersion and the ground-state density for $B = 7$ T are shown in Fig. 6. The electron density shows strong oscillations in the lateral direction. The maxima are formed in order to optimize the intralayer exchange energy. The width of each peak is nearly given by that of a single-particle state. It is determined by the short-range exchange interaction which, for a state with wave vector k, acts only in a region of $X_k - l_c < y < X_k + l_c$, with $l_c = [\hbar/(m^* \omega_c)]^{1/2}$, and $X_k = k l_c^2$ is the center coordinate of the state k. In order to minimize the interlayer Coulomb repulsion the density maxima in the two wires are shifted against each other. This gain in intralayer exchange and interlayer Hartree energy is at the cost of intralayer Hartree and interlayer exchange energy, as can be seen from Fig. 6(b). Only for certain k values are the single-particle states extended on both layers. This ground states resembles the CDW which was predicted for a 2DES.[13] It was predicted to form spontaneously for identical layers. In the case of quantum wires it is stabilized by the different confinement energies in the two layers.

The oscillatory behavior is also reflected in the subband dispersion. Local maxima and minima in the lowest subband correspond to symmetric and localized states, respectively. The reason for this is that the exchange for the localized states is stronger since it is due to intralayer exchange only, whereas for the symmetric states the exchange is partly due to the weaker interlayer interaction.

This CDW-like ground state evolves continuously from a state at $B = 4$ T which is very similar to that of Fig. 5. The amplitude of the density oscillations increases, until at $B = 6.4$ T the second subband is completely depopulated. Figure 7 shows the FIR absorption of this CDW in the range of $B = 6 - 7$ T. We find two modes which show an anticrossing at $B = 6.5$ T. We label these modes as ω_o (optical) and ω_a (acoustic). However, the situation is more complicated compared to the low-density case. As can be seen from Fig. 8, outside the anticrossing region the optical mode corresponds to an induced density which is out of phase. Since the ground-state densities are already out of phase, this corresponds to an in-phase center-of-mass motion of the densities in the two wires. Near the anticrossing the modes mix, and are mostly localized in either one of the wires (see Fig. 8). Due to the complicated subband structure and the induced density distribution, the origin of the anticrossing is very intricate. However, we regard it as a signature of the ground state which can be probed experimentally.

IV. SUMMARY

We have investigated the FIR absorption of different interaction-induced ground states of a pair of weakly coupled quantum wires at magnetic fields where one 1D subband is occupied. Similar to the 2D case, at small electron densities we find a coherent tunneling-dominated state, and at larger densities a state that has the characteristics of a CDW. We have shown that the FIR absorption is qualitatively different to that of a system that is only coupled by direct Coulomb interaction. The magnetic-field transition to the coherent state shows up in the spectrum as a jump in the energy of the acoustic mode which is found above that of the optical one. This can be explained by the enhanced tunneling gap. The CDW state shows a complicated subband structure which results in an anticrossing of the optical and acoustic mode around $\nu = 1$.

ACKNOWLEDGMENTS

This work was partially funded by the Deutsche Forschungsgemeinschaft through Grant No. He1938/6, the Graduiertenkolleg ''Physik Nanostrukturierter Festkörper,'' the Icelandic Science Foundation, and the University of Iceland Research Fund.

[1] S. Das Sarma and P. I. Tamborenea, Phys. Rev. Lett. **73**, 1971 (1994).
[2] R. J. Radtke, P. I. Tamborenea, and S. Das Sarma, Phys. Rev. B **54**, 13 832 (1996).
[3] L. Zheng, M. W. Ortalano, and S. Das Sarma, Phys. Rev. B **55**, 4506 (1997).
[4] L. Zheng, R. J. Radtke, and S. Das Sarma, Phys. Rev. Lett. **78**, 2453 (1997).
[5] S. Das Sarma, S. Sachdev, and L. Zheng, Phys. Rev. Lett. **79**, 917 (1997).
[6] T. Jungwirth and A. H. MacDonald, Phys. Rev. B **53**, 9943 (1996).
[7] K. Yang *et al.*, Phys. Rev. B **54**, 11 644 (1996).
[8] V. Pellegrini *et al.*, Phys. Rev. Lett. **78**, 310 (1997).
[9] H. C. Manoharan *et al.*, Physica E **1**, 172 (1997).
[10] A. S. Plaut *et al.*, Phys. Rev. B **55**, 9282 (1997).
[11] S. He, S. Das Sarma, and X. C. Xie, Phys. Rev. B **47**, 4394 (1993).
[12] T. Lay *et al.*, Phys. Rev. B **50**, 17 725 (1994).
[13] R. Côté, L. Brey, and A. H. MacDonald, Phys. Rev. B **46**, 10 239 (1992).
[14] J. J. Palacios and P. Hawrylak, Phys. Rev. B **51**, 1769 (1995).
[15] H. Aoki, Physica E **1**, 198 (1997).
[16] L. Świerkowski and A. H. MacDonald, Phys. Rev. B **55**, 16 017 (1997).
[17] O. Mayrock, S. A. Mikhailov, T. Darnhofer, and U. Rössler, Phys. Rev. B **56**, 15 760 (1997).
[18] C. Steinebach, D. Heitmann, and V. Gudmundsson, Phys. Rev. B **56**, 6742 (1997).
[19] E. Ulrichs *et al.*, Phys. Rev. B **56**, 12 760 (1997).
[20] C. Steinebach *et al.*, Phys. Rev. B **57**, 1703 (1998).
[21] V. Gudmundsson and A. S. Loftsdóttir, Phys. Rev. B **50**, 17 433 (1994).
[22] V. Gudmundsson and J. J. Palacios, Phys. Rev. B **52**, 11 266 (1995).